Texture analysis of optical coherence tomography speckle for characterizing biological tissues *in vivo*

Andras A. Lindenmaier,[1] Leigh Conroy,[1] Golnaz Farhat,[1,2] Ralph S. DaCosta,[1,3] Costel Flueraru,[4] and I. Alex Vitkin[1,3,5,*]

[1]*Department of Medical Biophysics, University of Toronto, 610 University Ave., Toronto, Ontario M5G 2M9, Canada*

[2]*Imaging Research, Sunnybrook Health Sciences Centre, 2075 Bayview Ave., Toronto, Ontario M4N 3M5, Canada*

[3]*Ontario Cancer Institute, University Health Network, 610 University Ave., Toronto, Ontario M5G 2M9, Canada*

[4]*Institute for Microstructural Sciences, National Research Council, 1200 Montreal Road, Ottawa, Ontario K1A 0R6, Canada*

[5]*Department of Radiation Oncology, University of Toronto, 610 University Ave., Toronto, Ontario M5G 2M9, Canada*

**Corresponding author: Alex.Vitkin@rmp.uhn.on.ca*

Received December 20, 2012; revised March 10, 2013; accepted March 11, 2013; posted March 12, 2013 (Doc. ID 182155); published April 5, 2013

We demonstrate a method for differentiating tissue disease states using the intrinsic texture properties of speckle in optical coherence tomography (OCT) images of normal and tumor tissues obtained *in vivo*. This approach fits a gamma distribution function to the nonlog-compressed OCT image intensities, thus allowing differentiation of normal and tumor tissues in an ME-180 human cervical cancer mouse xenograft model. Quantitative speckle intensity distribution analysis thus shows promise for identifying tissue pathologies, with potential for early cancer detection *in vivo*.

OCIS codes: 100.2960, 110.4500, 170.3880, 170.6935.

Cancer is a prevalent disease with terrible social and economic consequences. Early detection of cancer is crucial for timely intervention, which can lead to better outcomes [1]. Imaging methods that use light-tissue interactions have been shown to be sensitive to many subtle diseased tissue alterations [2]. As such, optical coherence tomography (OCT) is a promising technology that may play a role in the differentiation between normal and diseased tissue states *in situ*. It is particularly attractive for clinical application because of its high resolution, subsurface imaging capability up to ~2 mm in tissue and fiber optic implementation that permits minimally invasive access to many anatomically restricted areas. While OCT's impressive resolution is on the micrometer scale, this is generally insufficient for direct visualization of cellular organelles and cellular level changes, as these are submicrometer in size. There is, however, some evidence that image analysis of OCT speckle patterns can extract additional tissue information [3,4]. Speckle in OCT images results from the interference of backscattered light from the subresolution scatterers in the tissue being imaged. Speckle is known to give a good measure of the underlying scatterers' average properties, such as size, shape, and distribution, without individually resolving them [3].

In this study, we use the local variation in OCT speckle to obtain a measurement of the average changes in the scatterer properties of the tissue being imaged. The metric is then used to differentiate between normal and tumor tissues *in vivo*. Specifically, the spatial variation of OCT speckle intensities is quantified by fitting the uncompressed OCT data to a gamma distribution function, similar to methods used in previous high-frequency ultrasound tissue characterization studies and an OCT apoptosis study [5,6]. The pixel intensity distribution is approximated by the gamma distribution using a simple least squares optimization algorithm. The OCT speckle variation is quantified through the fit parameters of this distribution. To test this, *in vivo* OCT imaging was performed on NCr nude mice with dorsal skin-fold transparent window chambers (WCs) to allow for direct imaging of normal and solid tumor tissues [7]. Fluorescently labeled DsRed-Me180 cervical cancer xenografts were implanted in the mouse dorsal skin-fold WCs and monitored using OCT starting 7 days after implantation. This animal model permitted OCT imaging of tissues for up to 28 days from tumor cell implantation (which usually coincides with WC implantation). All animal studies were performed in accordance with University Health Network Animal Resource Center guidelines for the care and use of laboratory animals.

The OCT system used in this study has been described previously [8]. Briefly, it uses a 20 kHz Santec HSL2000-HL laser source with center wavelength at 1320 nm and bandwidth of 110 nm, resulting in an axial resolution of 7 μm in tissue. Using a 3×3 Mach–Zender interferometer with a semiconductor optical amplifier in the sample arm and dual channel simultaneous detection, the system allows for higher signal-to-noise ratio than conventional systems. A heater and translation stage were used to position the ketamine and xylazine anesthetized mice under the ball lens fiber of the OCT probe.

Representative B-mode OCT images were collected from within the tumor area as well as surrounding normal tissues in the WC. The tumor contour was visible directly in the OCT images, but as a definitive measure, the tumors were also imaged using a Leica MZ FLIII stereomicroscope (Leica Microsystems GmbH, Wetzlar, Germany) with a 560 nm excitation filter for localization of the Texas Red glowing tumors. This allowed each B-mode image to be categorized as being from a tissue region that is either normal, contoured tumor or in-between transition area. A region of interest (ROI) was then selected within each image (normal or tumor

tissue images), starting at a depth of 100 pixels below the top of the coverslip of the WC. The standard depth was chosen to minimize complicating effects due to signal attenuation with depth. The ROI was 64×190 pixels, corresponding to a physical size of $\sim 210\ \mu m \times 630\ \mu m$, chosen large enough to allow for good histogram statistics. The OCT pixel intensity distribution in the ROI (without log-compression) was then represented as a histogram. Various methods of optimizing the binning of the distribution, including fixed and "dynamic" binning based on the Shimazaki method [9] were tested; fixed binning was found to be optimal for histogram comparison of many images as this kept the relative histogram amplitudes constant and comparable between images. The histograms were then fitted using a least squares method with the gamma distribution function [10]:

$$f(x,\alpha,\beta) = \frac{1}{\Gamma(\alpha)}\beta^{\alpha}x^{\alpha-1}e^{-\beta x}. \quad (1)$$

The parameters α, β are known as the shape and scale parameter, respectively [5,10]. While individually they describe different aspects of the gamma distribution, the "mean" of the distribution obtained via α/β was used here as a composite metric for the detection of tissue properties. As described by Tunis *et al.* [5] in the context of high frequency ultrasound, the α/β ratio is proportional to the effective tissue scatterer number density, and can be related to cellular changes that affect the scattering properties of the tissue.

Representative histograms of nonlog-compressed OCT signal intensities are shown in Fig. 1 for a normal and a tumor region, showing clear differences in the distribution of speckle intensities and the α/β mean of the corresponding gamma fits varying accordingly. The goodness of fit was typically $R^2 \sim 0.985$ (range 0.950–0.990 for several hundred ROIs), demonstrating excellent quantitative description of the data. Figure 2(a) shows a representative B-scan image that encompasses the transition from a normal to a tumor region in the WC, while Fig. 2(b) shows the variation of the mean α/β parameter across the normal-tumor boundary. This was obtained based on a sliding box algorithm, similar to the one used for fractal box counting [11]. The algorithm slides a box, equal in size to the ROI of 64×190 pixels, from the left to the right of the image, calculating the mean α/β parameter

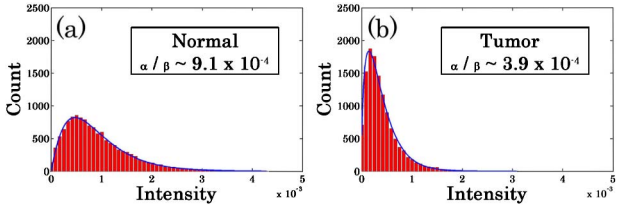

Fig. 1. (Color online) Histograms of the OCT image pixel intensity distribution in a 64×190 pixel ($\sim 210\ \mu m \times 630\ \mu m$) ROI region for (a) normal and (b) Me180 tumor tissue 17 days after tumor implantation. The mean α/β parameter was found by fitting the distribution with the gamma function [Eq. (1)], with the line of fit shown in blue. The mean α/β parameter values were found to be 9.08×10^{-4} and 3.94×10^{-4} for the normal and tumor tissue, respectively.

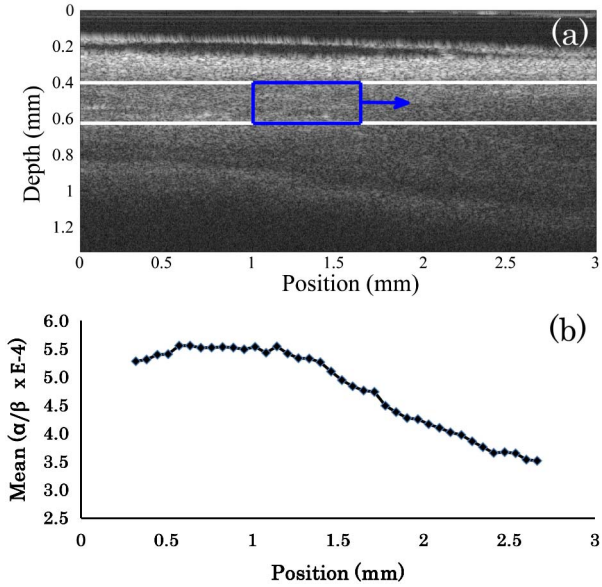

Fig. 2. (Color online) (a) B-mode image of normal to tumor tissue (left to right) transition region of a mouse 17 days postinjection of tumor cells. The 64×190 pixel ROI box is blue and its sliding region is shown by the white lines. The image field of view is 1.32 mm × 3 mm (depth × width). (b) The variation of the mean α/β parameter as a function of the center of the sliding ROI in (a).

in the ROI at every step. In the calculations of the data shown, the step size was 19 pixels (90% overlap of consecutive boxes) and the sampled area was at a depth of 120 pixels from the top of the image (i.e., ~100 pixels from top of the WC). The transition from normal to tumor regions is well quantified by the decrease in the α/β mean of the gamma distribution fits. Since the OCT image being analyzed is a transition region between normal and tumor tissue, the range of values of the α/β mean falls between the extremes of purely normal and purely tumor regions in Fig. 1. Similarly, when comparing images from different tissue regions in the WC, corresponding to both normal and tumor tissue, the strong correlation of the α/β mean parameter with disease state is also evident. Figure 3(a) shows the separation between normal, tumor, and "transition" regions (total of 52 images from 25 normal, 25 tumor, and 2 transition regions). The α versus β plot clearly classifies the tumor and normal tissue

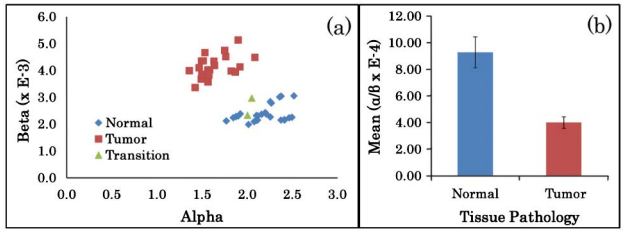

Fig. 3. (Color online) (a) Plot of the α/β ratio from ROIs of 52 images of varying origin: 25 normal, 25 tumor, and 2 transition regions of a mouse 17 days postinjection of tumor cells. The ROI used for the image analysis was 64×190 pixels and at a depth of 100 pixels below the top of the WC, as before. (b) Bar plot of the average α/β mean parameter from normal and tumor tissue. The error bars are ± 1 SD from the mean.

into two groups, while the transition regions of unknown/mixed tissue pathology fall somewhere in between, being similar to the normal tissue.

In Fig. 3(b) the average α/β mean parameter value is shown for sets of normal and tumor images. The resultant differentiation is excellent: using an unpaired two-tailed t-test it was determined that the difference between the two groups was statistically significant at a 95% confidence level with a p-value of $\sim 10^{-20}$. The variation within a given pathology is quite small, as shown by the modest size of the error bars ($\pm$ standard deviation). This suggests that the metric detects details of tissue microstructural variation that are finer than differences due to different tissue types, and is thus sensitive to subtle features of tissue heterogeneity. This quantifiable heterogeneity effect is considerably smaller than the tumor–normal tissue differences, and as such does not confound the differentiation of these tissue types.

Since the methodology enables the detection of small variations in tissue heterogeneity, the described speckle analysis technique could also be used for the detection of changes within a tissue type. For example, a common cancer treatment is radiation therapy. While the detailed radiobiology of tumors is still not completely understood [12], radiation-induced cell death, cellular structural changes, and connective tissue alterations may result in changes of the optical properties of tissues. As such, and based on the current findings, the response of tumors to radiation may potentially be monitored using the OCT speckle analysis algorithm described herein. Since OCT is noninvasive, and the mouse WC allows for focal irradiation of the tumor, the analysis pipeline could provide a valuable preclinical tool for the study of radiation response dynamics in solid tumors and adjacent normal tissues longitudinally and *in vivo*. In addition to fundamental insights, noninvasive detection of early radiobiological tissue alterations could be performed clinically using fiber optic technologies and thus used to guide adaptive radiation treatment delivery. Since clinical assessment of radiation response currently incurs delays of weeks to months, our proposed methodology could potentially enable earlier detection (~2–3 weeks) of tissue changes and corresponding treatment adjustments.

While the presented method was applied to 2D B-mode images, its use can be easily extended to the analysis of 3D datasets. By analyzing 3D data, the method can allow for the delineation of tumors and the sensitive volumetric mapping of tissue property variations.

A drawback of the current implementation of the method is its use of a relatively large ROI of 210 μm × 630 μm, as selected to get suitable gamma fits and statistics, which results in some spatial blurring and averaging over potentially heterogeneous tissue regions. Further systematic studies of ROI size/shape that will improve the method's spatial resolution and minimize averaging while still yielding accurate fits will likely yield better results. Such studies are ongoing. The α/β mean parameter shows good differentiation between normal and tumor tissue types, however it is not clear exactly what biological events are causing the changes in the speckle signal and the variation in intensity distributions. Correlative studies of tissue histopathology and two-photon fluorescence microscopy will be used to link variations in the α/β mean parameter to tissue- and cellular-level changes in the tissue. While the preliminary results presented here demonstrate promise for differentiating tissue types, additional metrics may be necessary to sample the subtle and complex spectrum of tumor tissue biology and response to treatments. With a multiparametric approach, the correlation of biological events to a biophysical metric parameter space may become realistic and useful. Further, the imaging optics (i.e., the NA, illumination geometry, working distance) may influence the performance of the algorithm, effects yet to be studied. Preliminary results from a different OCT system indicate comparable algorithm performance in differentiating normal from tumor tissue (data not shown), suggesting that the methodology is fairly robust.

In summary, we describe a novel quantitative OCT speckle analysis algorithm based on gamma distribution fits. We demonstrate its performance in differentiating between normal and tumor tissues *in vivo* in a WC mouse xenograft setting. The method has the potential for detecting subtle tissue alterations caused by disease development (e.g., cancer progression), or stemming from minimally invasive treatments (e.g., radiation therapy). In the former context, early tumor detection and staging/margin delineation may be possible; in the latter scenario, treatment feedback/personalization are attractive options. Several avenues for further studies and methodology improvement have also been outlined.

The authors thank Dr. Nataliya Portman (Montreal Neurological Institute) for the helpful discussions. This research was funded by the Natural Sciences and Engineering Research Council of Canada and the Canadian Institutes of Health Research.

References

1. R. Etzioni, N. Urban, S. Ramsey, M. McIntosh, S. Schwartz, B. Reid, J. Radich, G. Anderson, and L. Hartwell, Nat. Rev. Cancer **3**, 243 (2003).
2. V. Tuchin, *Tissue Optics: Light Scattering Methods and Instruments for Medical Diagnosis* (SPIE, 2007).
3. J. M. Schmitt, S. H. Xiang, and K. M. Yung, J. Biomed. Opt. **4**, 95 (1999).
4. K. W. Gossage, T. S. Tkaczyk, J. J. Rodriguez, and J. K. Barton, J. Biomed. Opt. **8**, 570 (2003).
5. S. Tunis, G. J. Czarnota, A. Giles, M. D. Sherar, J. W. Hunt, and M. C. Kolios, Ultrasound Med. Biol. **31**, 1041 (2005).
6. G. Farhat, V. X. D. Yang, G. J. Czarnota, and M. C. Kolios, J. Biomed. Opt. **16**, 026017 (2011).
7. A. Maeda, M. K. K. Leung, L. Conroy, Y. Chen, J. Bu, P. E. Lindsay, S. Mintzberg, C. Virtanen, J. Tsao, N. A. Winegarden, Y. Wang, L. Morikawa, I. A. Vitkin, D. A. Jaffray, R. P. Hill, and R. S. DaCosta, PLoS One **7**, e42133 (2012).
8. Y. Mao, C. Flueraru, S. Chang, D. P. Popescu, and M. G. Sowa, Opt. Commun. **284**, 2622 (2011).
9. H. Shimazaki and S. Shinomoto, Neural Comput. **19**, 1503 (2007).
10. J. A. Rice, *Mathematical Statistics and Data Analysis* (Duxbury Resource Center, 2007).
11. C. Allain and M. Cloitre, Phys. Rev. A **44**, 3552 (1991).
12. M. Joiner and A. van der Kogel, eds., *Basic Clinical Radiobiology*. (Hodder Arnold, 2009).